Dynamic behavior and onset of low-dimensional chaos in a modulated homogeneously broadened single-mode laser: Experiments and theory

J. R. Tredicce
Physics Department, Drexel University, Philadelphia, Pennsylvania 19104

F. T. Arecchi,* G. P. Puccioni,† A. Poggi, and W. Gadomski‡
Istituto Nazionale di Ottica, L. E. Fermi 6, 50125 Firenze, Italy
(Received 18 November 1985)

This is a detailed experimental study of the dynamical behavior of a CO_2 laser with modulated losses. We describe the observation of period-doubling transitions into chaos that are in good agreement with the predictions of the theory of one-dimensional maps and give examples of temporal evolutions, phase-space portraits, power spectra, and Poincaré sections. With the help of bifurcation diagrams we provide evidence for the appearance of generalized multistability. We also discuss the results of dimensionality tests that we have carried out on both our experimental data and corresponding numerical simulations based on the Maxwell-Bloch equations after the adiabatic elimination of the polarization. We conclude with an evaluation of the Kolmogorov entropy.

I. INTRODUCTION

During the last few years, numerous theoretical papers have shown the existence of self-pulsing instabilities and chaos in laser models.[1-3] Following a useful classification introduced in Ref. 4, we restate that only class-C lasers are capable, in principle, of the type of dynamical behavior described by the Lorenz equations.[5]

Here, instead, we offer a detailed treatment of the transition to chaos in a single-mode class-B laser.[4] The Maxwell-Bloch equations describing the interaction of N homogeneously broadened two-level atoms and a single-mode field in the slowly varying, amplitude approximation have the familiar form

$$\begin{aligned}\partial E/\partial t &= -i\omega_c E - gP - \kappa E \ , \\ \partial P/\partial t &= -i\omega_a P - gE\Delta N - \gamma_\perp P \ , \\ \partial \Delta N/\partial t &= 2g(EP^* + E^* P) - \gamma_{||}(\Delta N - \Delta N_0) \ ,\end{aligned} \tag{1}$$

where E is the complex field amplitude, P is the complex polarization, ΔN is the population inversion, and κ, $\gamma_\perp$, and $\gamma_{||}$ are their respective loss rates. ΔN_0 is the unsaturated population inversion, ω_c and ω_a are the cavity and atomic frequencies, respectively, and

$$g^2 = \omega\mu^2/\hbar\epsilon_0 V$$

is the coupling constant in terms of the transition dipole moment μ and the cavity volume V.

This model can be simplified when applied to a class-B laser, such as, for example, a CO_2 laser medium, where the pressure broadening provides a homogeneous gain line. A typical CO_2 laser system has a population relaxation time ($1/\gamma_{||} = 10^{-4}$ s) that exceeds by 4 orders of magnitude the duration of the decay of the polarization ($1/\gamma_\perp = 10^{-8}$ s); hence, the single-mode dynamics can be described accurately in the rate-equation approximation. On the basis of the inequality $\gamma_\perp \gg \kappa, \gamma_{||}$, we can solve the polarization equation in (1) under steady-state conditions and substitute the function $P(E, \Delta N)$ into the remaining equations (adiabatic elimination).[6]

The resulting two equations are insufficient to yield chaos. Different schemes have been proposed previously in order to increase the number of degrees of freedom of class-A or class-B systems.[7] The remainder of this paper will be devoted to a detailed investigation of a CO_2 laser with modulated losses on which we have already presented two preliminary reports.[8,9] We note, however, that our results apply also to a variety of other laser systems where the pump,[10] the cavity frequency,[11] or the $\gamma_\perp$,[12] are time-dependent parameters, as it was pointed out in Ref. 13.

The coupled field-molecule equations for a single-mode laser in resonance, after adiabatic elimination of the polarization, take the form

$$\begin{aligned}\partial S/\partial t &= -2\kappa(t)S + GS\Delta N \ , \\ \partial \Delta N/\partial t &= -\gamma_{||}(\Delta N - \Delta N_0) - 2GS\Delta N \ ,\end{aligned} \tag{2}$$

where $G = 2g^2/\gamma_\perp$, $S = |E|^2$, and $\kappa(t)$ is given by

$$\kappa(t) = \kappa_0[1 + m\cos(\Omega t)] \ . \tag{3}$$

Formally, the dynamical evolution can also be described by the three coupled equations

$$\begin{aligned}\partial S/\partial t &= -2\kappa_0(1 + m\cos Z)S + GS\Delta N \ , \\ \partial \Delta N/\partial t &= -\gamma_{||}(\Delta N - \Delta N_0) - 2GS\Delta N \ , \\ \partial Z/\partial t &= \Omega \ .\end{aligned} \tag{4}$$

In the absence of modulation $m = 0$, a linear perturbation analysis around the steady-state values

$$\begin{aligned}\Delta N_{st} &= 2\kappa_0/G \ , \\ S_{st} &= [(\Delta N_0/\Delta N_{st}) - 1]\gamma_{||}/2G\end{aligned}$$

yields a set of three eigenvalues λ_i

$$\lambda_1=0\ ,$$
$$\lambda_{2,3}=-(\gamma_{\parallel}C/2)\pm[(\gamma_{\parallel}C/2)^2-2\kappa_0\gamma_{\parallel}(C-1)]^{1/2}\ , \tag{5}$$

where $C=\Delta N_0/\Delta N_{st}$ is the so-called cooperation parameter.

In the case when $\gamma_{\parallel}$ is much smaller than κ_0, as in the CO_2 laser, the last two eigenvalues predict a linearized eigenfrequency $\Omega_0/2\pi$ of the form

$$\Omega_0/2\pi=[2\kappa_0\gamma_{\parallel}(C-1)]^{1/2}\ .$$

The heuristic picture[8] of a resonant destabilization of the system induced by a modulation process at a frequency Ω of the order of Ω_0 was confirmed in Ref. 13 even for very small values of the modulation depth. For typical CO_2 laser parameter values the linearized eigenfrequency is of the order of 200 kHz which is a very easily accessible frequency range for experiments.

In this paper we report detailed experimental and numerical studies of the temporal behavior of this system, its Poincaré sections, power spectra, and phase-space portraits of the entire bifurcation sequence. Phase diagrams in the parameter space give a clear picture of the destabilization process as a function of the various possible resonant frequencies, and the bifurcation diagrams indicate the existence of generalized multistability.

We have performed also dimensionality tests on the stroboscopic sections and on the time series constructed from our data and compared these results with the corresponding calculations based on the theoretical model. The comparison is very favorable and the data are in good agreement also with the general theory of nonlinear dynamical processes.

II. EXPERIMENTAL SETUP

The experimental setup is shown in Fig. 1. A grating with 97% efficiency selects only one line ($P20$) of the 10.6-μm band of the CO_2 laser. The beam expander (ratio 1:3) is inserted in the cavity to accommodate the electro-optic modulator (EOM) whose clear aperture is only 2 mm. Because the beam waist in the cavity is approximately 3.5 mm, it would be impossible to obtain laser action without the beam expander. The total operating pressure of the laser was varied from 13 to 20 Torr with partial pressures of about 75% He, 15% N_2, and 10% CO_2, while the current could be varied from 3 to 20 mA with a stability better than 0.1%. The entire system was also stabilized against thermal and vibrational disturbances. The driving unit of the EOM is an amplifier that can provide a bias voltage of 0—900 V from a stabilized high-voltage power supply and modulation amplitudes of up to 500 V peak to peak. The modulation function from a Rockland synthesizer is controlled in both amplitude and frequency by a Z-80A microprocessor and then amplified. The response of the driver is linear from 15 to 300 kHz, so that the voltage applied to the EOM can be trusted to be sinusoidal and to have a constant amplitude over the required range of frequencies. The axis of the EOM was set to 45° with relative to the direction of polarization set by the Brewster windows, with the result that the modulation affects only the cavity loss rate and not the optical path length or the cavity frequency.

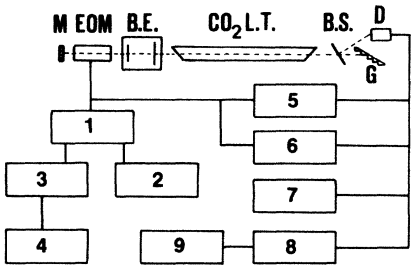

FIG. 1. Experimental setup. M, mirror; EOM, electro-optic modulator; B.E., beam expander; B.S., beam splitter; D, HgCdTe detector; G, grating; 1, amplifier; 2, high-voltage power supply; 3, frequency synthesizer (Rockland); 4, Z-80A microprocessor; 5, two-channel oscilloscope; 6, x-y oscilloscope; 7, spectrum analyzer (Rockland); 8, transient digitizer (Le Croy); 9, computer (HP1000).

The x-y oscilloscope is used to obtain the phase-space portrait (laser intensity L versus voltage applied to the EOM V). The real-time spectrum analyzer has a maximum frequency of 100 kHz. The LeCroy transient recorder (100-MHz bandwidth and maximum sampling rate, 32 000 samples) digitizes the signal and sends it to an HP1000 computer for dimensionality and entropy tests.

For selected measurements, such as bifurcation diagrams and Poincaré sections, we used a slightly different experimental arrangement than shown in Fig. 1.

The transmission function of the EOM has the form

$$S=S_0\cos^2(\pi V/V_{\pi/2})\ , \tag{6}$$

where S_0 is the input intensity, V is the voltage applied to the EOM, and $V_{\pi/2}$ is the voltage required to change the field polarization by 45° on a single pass through the EOM. The nonlinear transmission introduces strong superharmonic components in the laser response.

III. EXPERIMENTAL RESULTS

One of the main results obtained with this system is the observation of a period-doubling bifurcation sequence that leads to deterministic chaos. In Fig. 2 we report four different experimental tests to confirm that this is a true transition to chaos, namely: time behavior of the laser intensity, phase-space portraits, power spectra, and Poincaré sections. These data were collected at a constant modulation frequency ω and loss rate bias k_0, and by increasing the modulation amplitude m which acts as the control parameter. The presence of subharmonic bifurcations is clearly seen from the time series and power spectra. After a first sequence of three period-doubling bifurcations ($f/2$,$f/4$,$f/8$) we reach chaos and observe a broad-band power spectrum. A further increase in the modulation depth causes the system to enter a periodic window with a frequency $f/3$ [Fig. 3(a)] and after a new subharmonic bifurcation ($f/6$) [Fig. 3(b)], the system enters a second chaotic region. Up to this point, the whole dynamic response of the system is reminiscent of an ordinary Feigenbaum sequence. However, if we continue to in-

crease the control parameter, higher-order periodic windows of an even type begin to appear, such as, for example, $f/4$, $f/8$, and $f/6$ [Figs. 3(c) and 3(e)]. These are clearly different from what is observed at a smaller modulation amplitude and they do not seem to be predicted by a simple logistic map. As we shall see below, these bifurcations could correspond to the interaction of the subharmonic frequency with subharmonic components of the relaxation oscillation frequency.[13,14]

The low level of noise in the system is demonstrated by our observation of higher-order periodic windows including $f/7$ and $f/10$ [Fig. 3(f)] which are usually too narrow to be digitized. We believed that these windows have been observed experimentally for the first time in a laser system.

The phase-space portraits for the different subharmonic frequencies show that the maximum value of the intensity peaks increases when the modulation depth increases and their peak value is reached when the voltage applied to the EOM is closed to its minimum value. This was also observed during the first subharmonic sequence and it is expected because the minimum voltage leaves the cavity in the highest Q conditions which would lead to the maximum output of a steady-state laser. In the chaotic region the signal is aperiodic but its maximum intensity level is limited. We note, further, that although the leading edge of the pulses evolves in a nonpredictable way, the trailing edge has always the same shape as shown by a clear cutoff in the time traces and by a dense line on the phase-space portraits.

A stroboscopic measure of the intensity (in essence, a Poincaré section projected onto a single axis) is presented also in Fig. 2 and was taken using the period of the external modulation as a clock for the transient digitizer. This

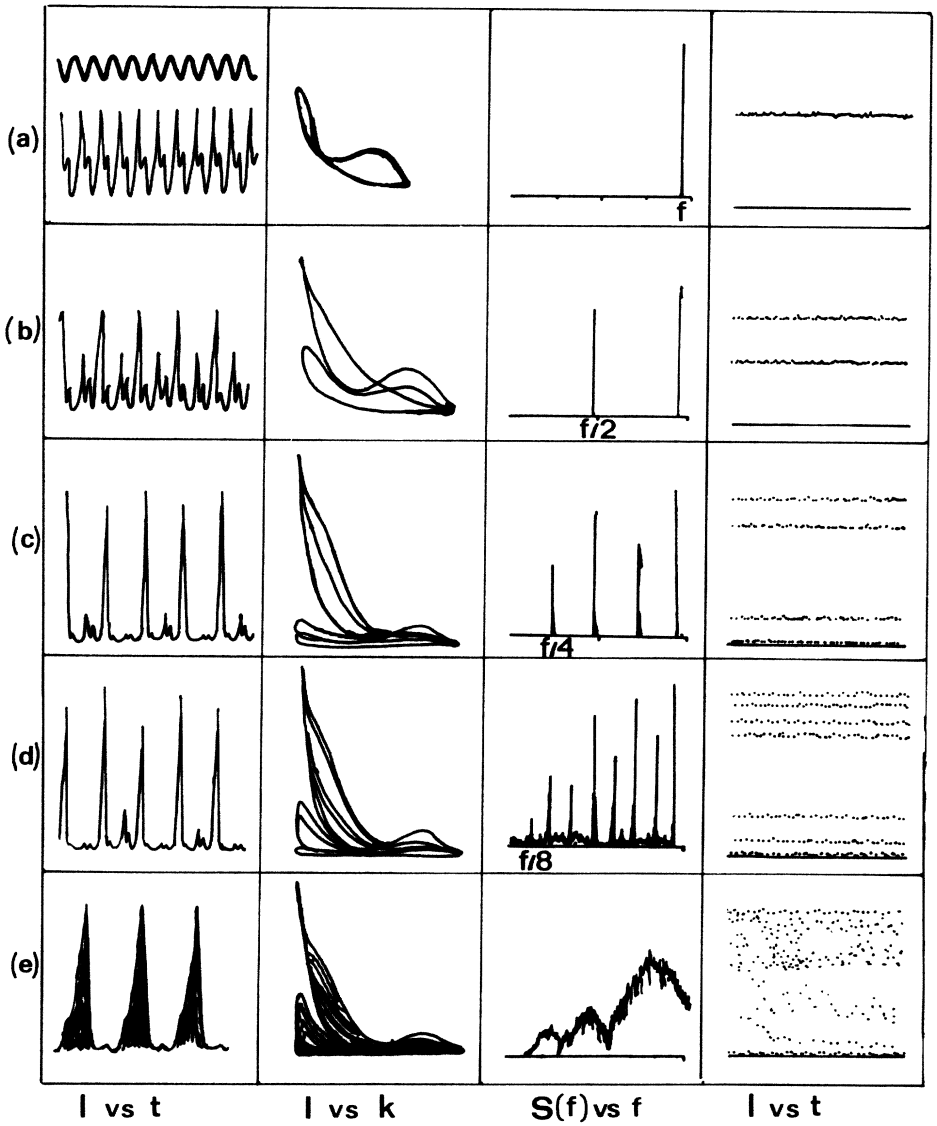

FIG. 2. Subharmonic sequence leading to chaos. From left to right: laser intensity as a function of time, phase-space plot, power spectrum, and stroboscopic section for (a) f (fundamental frequency), (b) $f/2$, (c) $f/4$, (d), $f/8$ subharmonic, and (e) chaotic behavior.

type of measurement opens the possibility of analyzing a very large number of periods (up to a maximum of 32 000) as opposed to the typical 800 which we would obtain by collecting 40 samples per period. Furthermore, it allows a much larger bandwidth in the processing of sequences of narrow pulses, otherwise requiring a high sampling rate with the related problems in data storing and processing.

From the stroboscopic sections, we have constructed return maps, such as shown in Fig. 4, which indicate that the sequence of bifurcations leading to chaos can be described quite well by a logistic map. This behavior has been observed by moving through the parameter space along a straight line that corresponds to a fixed frequency and variable modulation amplitude as indicated in Fig. 5(a).

In order to explore the behavior of the system in different regions of the parameter space, we scanned the frequency for different values of the modulation amplitude. The scans were controlled by the Z80 microprocessor, using a sweep rate that was several orders of magnitude smaller than the frequency of the external modulation and preserving the phase.

In Fig. 5(a) we have traced the boundaries between regions of different subharmonic behavior while the dc loss rate k_0 at its minimum value (no bias voltage applied to the EOM). Under these conditions the appearance of

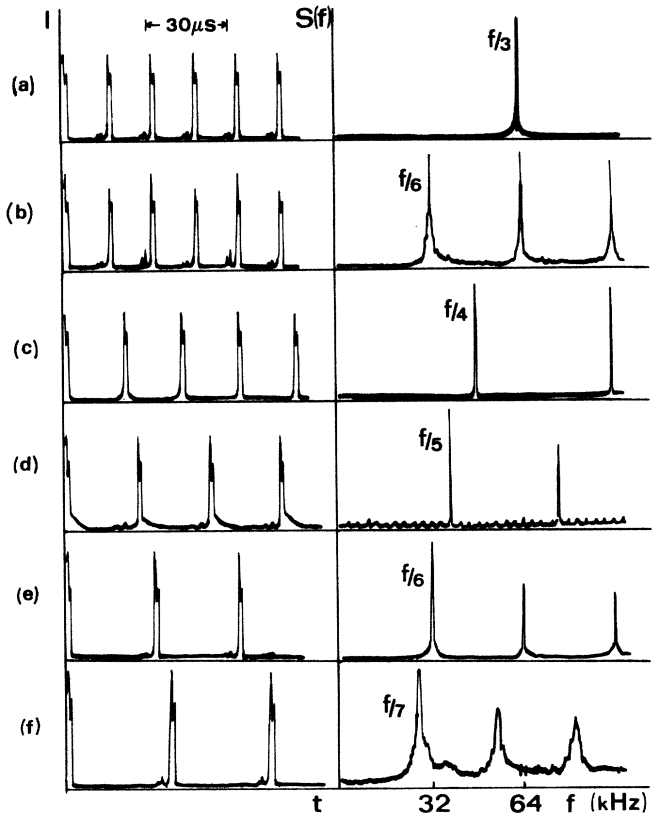

FIG. 3. Periodic windows inside the chaotic region. Laser intensity I as a function of time (left side) and power spectrum (right side) for: (a) $f/3$, (b) $f/6$, (c) $f/4$, (d) $f/5$, (e) $f/6$, and (f) $f/7$ subharmonics. Each periodic window after the first $f/6$ subharmonic is separated by a chaotic region.

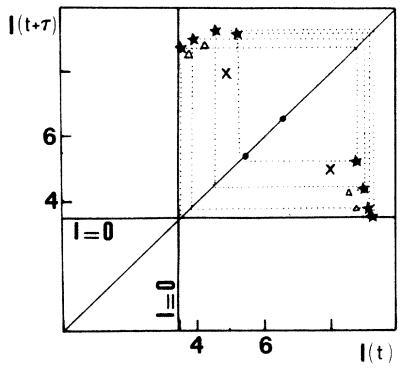

FIG. 4. Return map $I(t+\tau)$ vs $I(t)$, where τ is the modulation period, for different periodic solutions: ●, f; ×, $f/2$; △, $f/4$; *, $f/8$ of the period-doubling sequence. The two (●) correspond to two f solutions taken for different modulation amplitudes. The points corresponding to the $f/4$ and $f/8$ subharmonics fit a logistic map if we take into account that the axis of the map are displaced from the axis corresponding to zero intensity.

subharmonic components and the transition to chaos occur for modulation depths greater than 2% in a very narrow range of modulation frequencies between 190 and 192 kHz; this result is in qualitative agreement with the physical interpretation of a resonant destabilization due to the interaction between the modulation and the relaxation

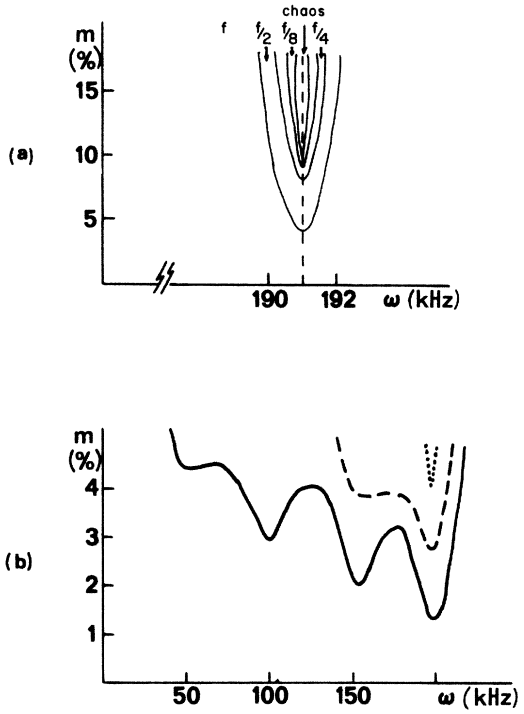

FIG. 5. Phase diagrams in the parameter space [m (modulation amplitude), ω (modulation frequency)]. (a) For the minimum value of k_0 ($V_{\text{bias}}=0$), we show the boundaries between different subharmonic bifurcations. (b) For different values of k_0, we show the boundaries between the f and $f/2$ subharmonic. Dotted line shows $k_0\min(V_{\text{bias}}=0\text{ V})$, dashed line shows $k_0'(V_{\text{bias}}=100\text{ V})$, and solid line shows $k_0''(V_{\text{bias}}=200\text{ V})$.

oscillation frequencies.

When k_0 is increased, by applying a bias voltage to the EOM, the required modulation depth is smaller, indicating that in this case the region of instability is broadened when the laser operates near threshold. This is especially clear in Fig. 5(b) where we show the boundary for the appearance of the first subharmonic component for different values of the bias voltage; it is clear that the requirements on m decrease on increasing k_0 and, in addition, we see a net broadening of the frequency regions over which the dynamic behavior becomes complicated. It is also clear that other resonant frequencies appear at lower thresholds for complicated behavior and they correspond to subharmonics (or harmonics of subharmonics) frequencies of the relaxation oscillation frequency. We see that the most resonant case (minimum value of m) occurs when the modulation frequency matches the frequency of the relaxation oscillations.

It is worth noticing that the boundaries between different kinds of attractors in Fig. 5 are only drawn qualitatively because of the appearance of generalized multistability[8,10–12] which gives different results for the curves shown in Fig. 5, as we pass through a limit between two subharmonic bifurcations by increasing or decreasing the frequency. In some cases for the same set of control parameters (k_0,m,ω) it is possible to observe as many as four different attractors depending on the initial conditions. The reproducibility of these effects and the possibility of separating the solutions allow us to confirm that these are deterministic effects rather than effects due to noise, as the general theory on nonlinear dynamics predicts.[14] Furthermore, and also due to the low amount of random noise that is present in our system, we found different attractors whose domain of attraction in parameter space is reduced to very narrow regions only a few hertz wide, resulting in a very complex structure that we have called "microstructure." In Table I we observe that a change of one part in 10^5 in frequency produces a jump among different attractors. The final state, thus, depends on the previous history.

These effects make it impossible to determine the phase boundaries in parameter space quantitatively, and even though some recent examples were shown,[15,16] we believe that in those cases noise averaging over the different possible attractors gives a blurred picture of the more complicated noise-free experimental behavior.

We have already mentioned the existence of generalized multistability which can be easily observed with the help of bifurcation diagrams. In Fig. 6 we show the peak intensity as a function of m for constant values of k_0 and ω. Results for increasing [Fig. 6(a)] or decreasing m [Fig. 6(b)] differ substantially.

From these diagrams it has been possible to evaluate the Feigenbaum universal constant δf. The result obtained after two bifurcations is $\delta f = 3.7 \pm 0.2$, which differs from the value 4.669... predicted asymptotically by the theory. Of course, δf is defined only in the asymptotic limit so that is not surprising that there should be some disagreement with the calculated value from our experiment, where the maximum observable subharmonic was $f/8$.

TABLE I. Modulation amplitude $=0.12$.

Modulation frequency (kHz)	Behavior
191.270	Chaos
191.290	$f/5$ or $f/4$
191.310	$f/3$ or $f/4$
191.320	$f/2$ or f
191.324	f
191.327	$f/2$ or $f/3$
191.331	$f/3$
191.337	$f/3$ or $f/4$
191.348	$f/4$ or $f/5$
191.480	$f/3$
191.600	Chaos
191.755	$f/3$
191.800	$f/6$
192.000	$f/2$ or chaos
192.190	Chaos
192.256	$f/4$ or $f/3$

Other remarks can be offered after a direct observation of the bifurcation diagram shown in Fig. 6. With increasing control parameter after a sequence of bifurcations, the system, for high values of m, cannot follow the modulation and jumps into a stable steady state for which no lasing action is obtained. Then the zero-intensity solution was stabilized by the modulation in very narrow regions of the parameter space indicating that this also is a

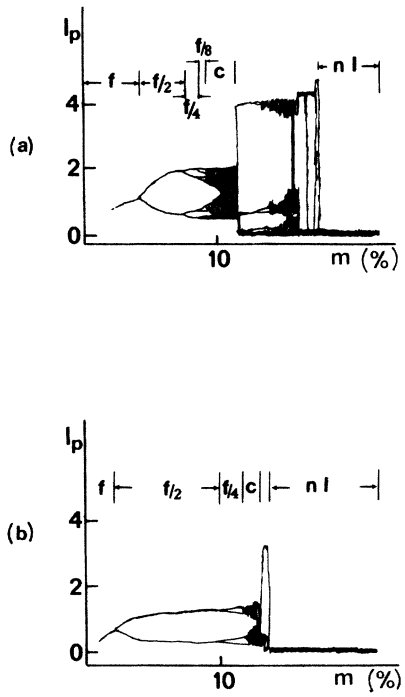

FIG. 6. Bifurcation diagrams. Peak intensity I_p as a function of the modulation amplitude m: (a) increasing m, (b) decreasing m. Generalized multistability and hysteresis of the nonlasing (nl) regions are shown.

resonant effect. After reaching this point and then reducing the modulation depth, the region where the zero-intensity solution is stable enlarges and when the intensity finally becomes different from zero the sequence of bifurcations looks completely different.

Thus far, we have shown the existence of subharmonic bifurcations and aperiodic behavior from the time series, power spectra, and Poincaré sections. However, the assertion that the system displays deterministic chaos cannot be justified until a clear distinction is made between the aperiodic signals and random noise. Several authors[17,18] have recently discussed the possibility of distinguishing turbulence from noise; it is well known, for example, that deterministic chaos in low-dimensional systems must show a low fractal dimension in contrast to noisy signals. Each strange attractor is characterized by a dimension which must be smaller than that of the phase space of the system. If there is a correspondence between the model described in the Introduction and our experimental results, we would expect that a dimensionality test on a chaotic signal would display a low (smaller than three) fractal dimension.

In Fig. 7 we plot the logarithm of the number of pairs of vectors in the embedded space whose distance is less

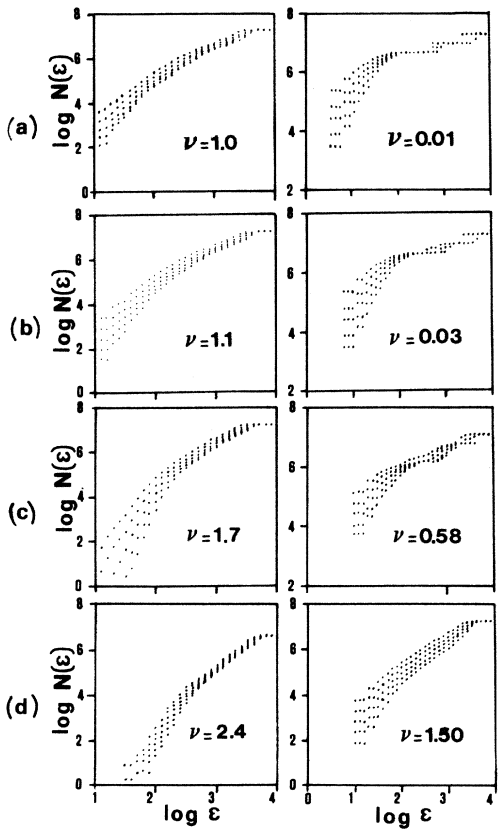

FIG. 7. Plots of $\log N_n(\epsilon)$ as a function of $\log\epsilon$ for different values of embedding dimension n calculated from the time series (left) and from the stroboscopic section (right) for different subharmonic bifurcations: (a) $f/2$, (b) $f/4$, (c) $f/8$, (d) chaotic behavior. The best fit values of the slope ν are calculated over an interval almost one decade large and are assumed to have an average estimated error ± 0.1.

than $\epsilon(\log N(\epsilon))$ as a function of the logarithm of ϵ for different values of the embedding dimension n. In the scaling region, we have $N_n(\epsilon)\sim\epsilon^{\nu}$ where ν is the information dimension of the attractor and it will be represented by the slope of those graphs independent of the embedding dimension.

For very small values of ϵ, the result is highly influenced by noise, while for very large ϵ, we observe a saturated region where $N(\epsilon)$ is constant. Of course, we are interested on the intermediate region where the complex structure of the strange attractor, if it exists, will be made especially clear. In Figs. 7(a)—7(c) we show the dimensionality tests performed on time series and stroboscopic sections corresponding to spectra with $f/2$, $f/4$, and $f/8$ subharmonic frequencies, respectively. As the solutions are periodic, the slopes obtained for $f/2$ and $f/4$ solutions saturate at $\nu=1$ in the time series and $\nu=0$ in the Poincaré sections. For the $f/8$ subharmonic ν is slightly above 1.5 [Fig. 7(c)]. In Ref. 9 we gave an heuristic interpretation of these results, claiming that the measured dimension for the $f/8$ subharmonic corresponds to the dimension at the accumulation point of a Feigenbaum cascade. For the chaotic region shown in Fig. 7(e), the fractal dimension jumps to a higher value ($\nu=2.4$).

The correlation entropy K_2 as a function of the embedding dimension n was nearly 0 for periodic solutions, with a maximum deviation of 30 Hz. This deviation from the theoretical value is typical of the error that can be associated to the measurement. For a chaotic solution, K_2 acquires a finite value ($\cong 40$ kHz) which is much greater than the 30-Hz maximum measured for a periodic solution.

As long as the dimension is smaller than three, it is reasonable to think that the model described in the introduction holds. In such a case, we have a single positive Lyapunov exponent (λ^+) which is of the order of K_2. With the help of the Kaplan and Yorke formula[19] we estimate the negative Lyapunov exponent (λ^-) as follows:

$$|\lambda^-| = \frac{\lambda^+}{\nu-2} \cong 100 \text{ kHz} .$$

Finally, three other experimental results can be pointed out.

(1) In the presence of a broadband spectrum, we detected three different kinds of temporal behavior. One corresponds to Fig. 2(e) for which the dimensionality test was performed [Fig. 7(d)]; as we noted above, these oscillations display a clear peak intensity limit. For different parameter values, a second kind of chaotic behavior can be found where the maximum peak intensity is much higher and the pulses are very narrow (<100 ns) [Fig. 8(a)] and the characteristic dimension grows to 2.1 in the Poincaré section which corresponds to 3.1 in the phase space [Fig. 8(b)]. In Fig. 9 we represent the third kind of signal corresponding to a broadband spectrum; this appears to be completely aperiodic when a large number of periods is observed. An expanded view, however, shows the existence of laminar periods corresponding to different subharmonics of the fundamental frequency ($f, f/2, f/6$ in the example) with sudden uncorrelated jumps between them. In this case, it is already necessary to determine if

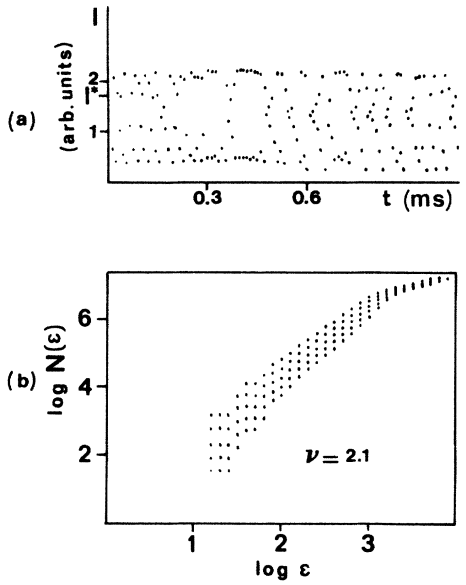

FIG. 8. Chaotic behavior in a region of high dimensionality: (a) stroboscopic plot of laser intensity as a function of time, (b) plot of $\log N_n(\epsilon)$ as a function of $\log(\epsilon)$. The value of I^* represents the maximum intensity observed in the chaotic region of Fig. 2(e). The value of ν given in (b) corresponds to the stroboscopic section and it is equivalent to 3.1 on the time series.

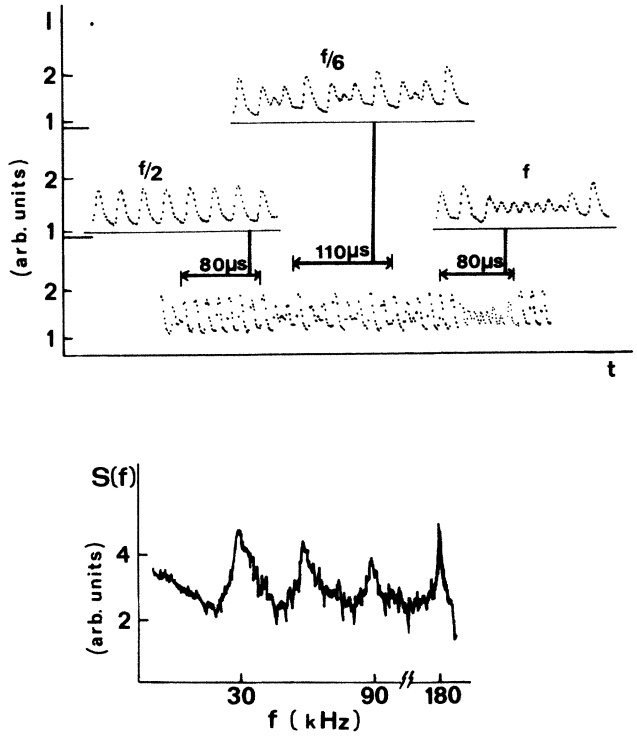

FIG. 9. Top: laser intensity as a function of time in a multistable region. The expanded figures show the three different attractors which are present in the signal. Bottom: broadened power spectrum of the signal.

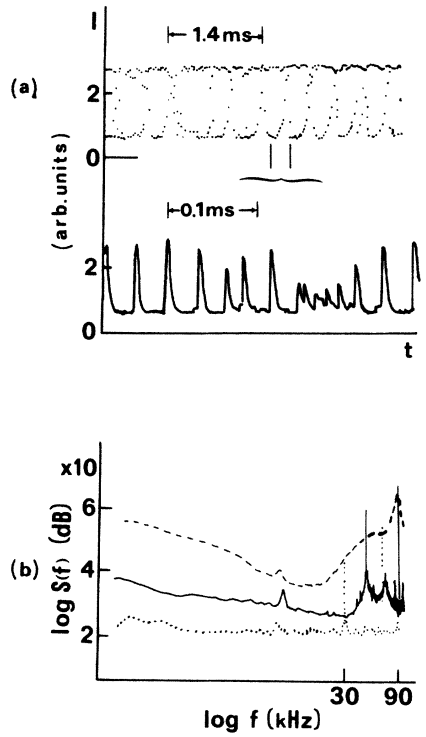

FIG. 10. (a) Laser intensity as a function of time in the region of intermittency, with an expanded view of the aperiodic behavior between two laminar periods. (b) Power spectra for an $f/6$ subharmonic (dotted), for the intermittency with the characteristic low-frequency divergence (dashed), and for the region above intermittency with a broadened $f/4$ subharmonic (solid line).

the jumps are due to the existence of noise or to an intrinsically deterministic behavior coming from an intermittent process.

(2) In a very narrow region of the parameter space, we found a periodic window with frequency $f/3$ which bifurcates giving an $f/6$ subharmonic component [Figs. 3(a) and 3(b)]. A further increase in modulation depth seems to produce a transition to chaos by intermittency as we show in Fig. 10(a) and to produce a low-frequency tail in the power spectrum [Fig. 10(b)] as predicted by the theory.[20]

(3) For high modulation amplitudes and very narrow regions of the modulation frequency, there is a stable zero-intensity solution with a large hysteresis. It is worth to stress that the zero-intensity solution is not due to the large value of k. In fact if one increases the modulation amplitude the laser action starts again.

IV. NUMERICAL RESULTS

By numerical integration of Eq. (4), we were able to reproduce the experimental results. We show in Fig. 11, a transition to chaos via subharmonic bifurcations similar to that shown in Fig. 2. Furthermore, for different initial conditions, but fixed values of m and ω, we found different attractors (Fig. 12); this is the evidence of generalized multistability as discussed in the experimental sec-

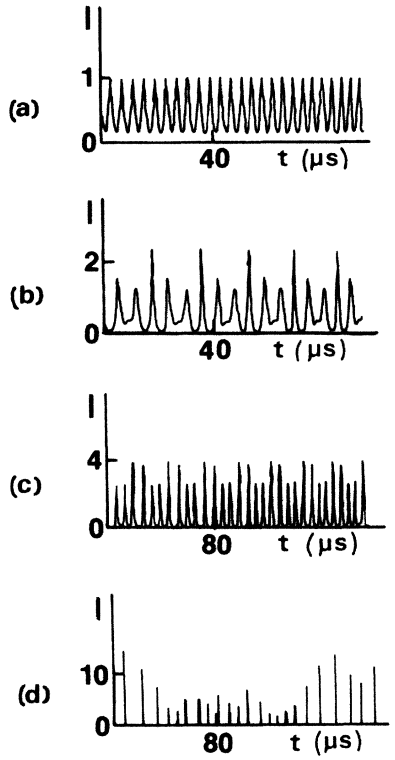

FIG. 11. Laser intensity as a function of time obtained by numerical integration of Eq. (4): (a) f (fundamental frequency), (b) $f/4$ and (c) $f/8$ subharmonic, (d) chaos.

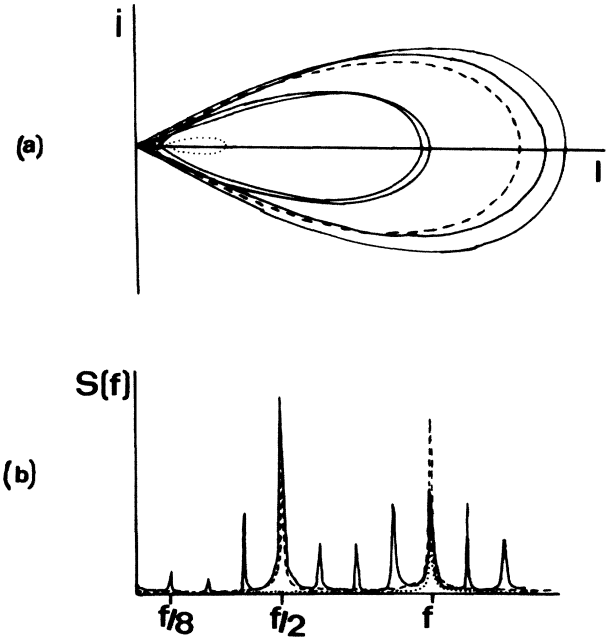

FIG. 12. Numerical results: (a) phase-space portrait ($\dot{I}$ vs I) and (b) power spectrum showing generalized multistability. A different set of initial conditions causes the system to fall on different attractors: Dotted line shows f, dashed line shows $f/2$, and solid line shows $f/8$, for the same parameter values.

tion. Alternatively, if we change the parameter values by very small amounts (e.g., one part in 10^4) the solution can display a different behavior, in agreement with the expected presence of microstructure.

We have also processed the numerical time series in the same manner as done with the experimental signal and obtained the dimension of the attractors. The results showed in Ref. 9 are in quantitative agreement with those of Fig. 7.

V. CONCLUSIONS

We have shown the existence of a period-doubling transition to chaos, intermittency, generalized multistability, and microstructure in the parameter space of a quantum optical system. All these phenomena can be explained in terms of a simple model based on the rate equations for a two-level system. Dimensionality tests and the calculation of the Kolmogorov entropy indicate that our experiment has a new feature relative to previous ones, insofar as, for the first time, we find a strict quantitative correspondence between the experimental chaos measured in the laboratory and the theoretical chaos provided by the model. The calculation of the negative Lyapunov exponent let us conclude that the relevant contraction rate, in phase space, is much smaller than the decay rate of the polarization so that it does not play a relevant role on the dynamics of the system.

In very narrow regions of the parameter space we found that the dimension measured from the experimental data is larger than three. In this case the dynamic behavior cannot be described by our simple model for large values of the modulation amplitude. Perhaps it is necessary to include the polarization. In fact, a reduction on the fractal part of the dimension ν indicates that a larger negative Lyapunov exponent, as it is expected coming from the polarization, plays a relevant role on the calculation of ν. This is the first time that information about the limits of validity of a theoretical model can be extrapolated from the calculation of the dimension of a strange attractor. Further work is still necessary to understand the physical origin of the generalized multistability, as well as the stabilization of the zero-intensity solution for high values of the modulation depth.

ACKNOWLEDGMENTS

We wish to thank N. B. Abraham, G. L. Lippi, and L. M. Narducci for helpful discussions and a careful reading of this paper. This work was supported in part by CODEST under European Joint Project on Optical Bistability.

*Also with University of Florence, Physics Department, Florence, Italy.
†Present address: Physics Department, University of Toronto, Toronto, Canada.
‡Present address: University of Warsaw, Warsaw, Poland.

[1]A. Z. Grazyuk and A. N. Oraevskii, in *Quantum Electronics and Coherent Light,* edited by P. A. Miles (Academic, New York, 1964), p. 192.
[2]H. Haken, Phys. Lett. **53A**, 77 (1975).
[3]For an overview see, e.g., N. B. Abraham, L. A. Lugiato, and L. M. Narducci, J. Opt. Soc. Am. **B2**, 7 (1985), and references therein.
[4]J. R. Tredicce, F. T. Arecchi, G. L. Lippi, and G. P. Puccioni, J. Opt. Soc. Am. **B2**, 173 (1985).
[5]Recent works on far-infrared lasers have shown the existence of instabilities, see, e.g., N. B. Abraham, D. Dangoisse, P. R. Glorieux, and P. Mandel, J. Opt. Soc. Am. **B2**, 23 (1985); C. O. Weiss, W. Klische, P. S. Ering, and M. Cooper, Opt. Commun. **52**, 408 (1985). An interpretation of these instabilities, however, as derived from the Lorenz model, requires further work due to complexity of the energy level diagram and the atomic interaction with the pump.
[6]H. Haken, *Synergetics—An Introduction,* 3rd ed. (Springer-Verlag, Berlin, 1983).
[7]F. T. Arecchi, G. L. Lippi, G. P. Puccioni, and J. R. Tredicce, Opt. Commun. **51**, 308 (1984), and references therein.
[8]F. T. Arecchi, R. Meucci, G. P. Puccioni, and J. R. Tredicce, Phys. Rev. Lett. **49**, 1217 (1982).
[9]G. P. Puccioni, A. Poggi, W. Gadomski, J. R. Tredicce, and F. T. Arecchi, Phys. Rev. Lett. **55**, 339 (1985).
[10]W. Klische, H. R. Telle, and C. O. Weiss, Opt. Lett. **9**, 561 (1984).
[11]T. Midavaine, D. Dangoisse, and P. Glorieux, Phys. Rev. Lett. **55**, 1989 (1986).
[12]E. Brun, B. Derighetti, D. Meier, R. Holzner, and M. Ravani J. Opt. Soc. Am. **B2**, 156 (1985).
[13]J. R. Tredicce, N. B. Abraham, G. P. Puccioni, and F. T. Arecchi, Opt. Commun. **55**, 131 (1985). I. I. Matorin, A. S. Pikovskii, and Ya. I. Khanin, Sov. J. Quantum Electron **14**, 1401 (1984).
[14]N. Minorski, *Nonlinear Oscillations* (Princeton University Press, Princeton, 1962).
[15]C. O. Weiss, A. Godone, and A. Olafsson, Phys. Rev. A **28**, 892 (1983).
[16]L. M. Hoffer, T. H. Chyba, and N. B. Abraham, J. Opt. Soc. Am. B **2**, 102 (1985).
[17]P. Grassberger and I. Procaccia, Phys. Rev. A **28**, 2951 (1983).
[18]J. D. Farmer, E. Ott, and J. Yorke, Physica (Utrecht) **7D**, 153 (1983).
[19]J. L. Kaplan and J. A. Yorke, *Lecture Notes in Mathematics,* edited by H. O. Peitgen and H. O. Walther (Springer, Berlin, 1980), Vol. 730, p. 228.
[20]Y. Pomeau and P. Manneville, Commun. Math. Phys. **74**, 189 (1980).